Iraqi Geological Journal

Journal homepage: https://www.igj-iraq.org

Petrophysical Evaluation of the Zubair Formation's Main Pay Zone Using Conventional and NMR Log Data: Insights from the North Rumaila Field, Southern Iraq

Ali Z. Abdullah[1*], Amna M. Handhal[2] and Rasha A. Al-Ali[3]

1 Department of Geology, College of Science, University of Basrah, Basrah, Iraq
* **Correspondence:** Alizuhair095@gmail.com

Received: 17 October 2024
Accepted: 17 February 2025
Published: 30 April 2025

Abstract

This study investigates the calculation of petrophysical properties using both conventional logging tools and Nuclear Magnetic Resonance logs for the main pay zone of the Zubair Formation, Recognized as one of the most significant hydrocarbon-producing formations in the North Rumaila Field, located in southern Iraq, the main pay zone is categorized into three permeable units (AB, DJ, and LN) and two impermeable isolated zones (C and K) based on log responses. The petrophysical analysis of these zones indicates that the shale volume increases toward the northern part of the field due to the depositional environment. Effective porosity values across these zones range from fair to good; however, some wells in the AB layer exhibit excellent porosity, notably wells X-7, X-62, X-83, and X-110. Additionally, hydrocarbon saturation levels remain consistently high in the AB and DJ layers, whereas certain wells in the LN layer display lower saturation values, particularly wells X-85, X-78, X-63, X-110, X-84, X-19, and X-115. Furthermore, permeability values were calculated using the KSDR equation based on Nuclear Magnetic Resonance logs that span from good to very good, except well X-115, demonstrating excellent permeability in the AB layer.

Keywords: North Rumaila field; Zubair Formation; Nuclear Magnetic Resonance; Porosity; Permeability

1. Introduction

Petrophysics is the study of porous media, specifically reservoir rocks and the fluids they contain, as well as their fundamental chemical and physical properties (Macini and Mesini, 2008). Petrophysical characteristics are essential for the ability of hydrocarbon reservoirs to store and yield profitable hydrocarbon resources. These characteristics, such as porosity, permeability, water saturation, lithology, and shale volume, are crucial for reservoir study. Porosity, which describes the volume of voids inside a rock directly influences its capacity to hold fluids such as water, gas, or oil (Hasoon and Farman, 2024).Well logging plays a crucial role in petrophysical log interpretation and geological decision-making, lithological determination and petrophysical characteristics calculation (Liu, 2017).

In this study, we analyze and interpret a variety of open-hole well logs, including conventional logs such as resistivity, porosity, and gamma-ray logs, as well as advanced logs such as Nuclear Magnetic Resonance (NMR). The data derived from these logs provide a comprehensive analysis and deeper understanding of the petrophysical characteristics essential for evaluating reservoir units. This evaluation includes the calculation of shale volume and porosity, along with the estimation of

hydrocarbon saturation. By thoroughly assessing these properties, it becomes possible to predict the performance of the reservoir units and their potential for hydrocarbon production.

The present study focuses on the Zubair Formation, with wells selected to cover most areas of the North Rumaila field, one of the largest and most significant oil fields in southern Iraq, located approximately 50 kilometers west of Basra city. The upper and lower boundaries of the Zubair Formation were identified, and the formation was divided into three permeable zones and two impermeable zones based on log responses, particularly gamma ray (GR) and spontaneous potential (SP) logs. Furthermore, the petrophysical characteristics of the formation were calculated providing crucial insights into the reservoir's properties. These detailed analyses not only enhance our understanding of the reservoir's potential but also contribute to more effective reservoir management strategies and optimized hydrocarbon production.

2. Geological Settings

The North Rumaila oil field is located approximately 53 km west of Basra city, between longitudes 46°14'14"E and 47°26'14"E and latitudes 30°55'7"N and 31°12'14"N (Jaffar, 2018). It is a double-plunging simple, and asymmetrical anticline with the long axis trending northeast (Fig. 1).

The focus of this study is the Rumaila field, which is located within the unstable Iraqi shelf inside the lower Mesopotamia zone (Sissakian, 2013). The Mesopotamian Zone is divided into three main subzones, the Tigris Subzone in the northeast, the Euphrates Subzone in the west, and the Zubair Subzone in the south (Abdulnaby, 2019). The Zubair Subzone is bounded by the Takadid-Qurna transversal fault to the north and the Al-Batin fault to the south (Almayahi and Ajeel, 2020). Two domes, South Rumaila and North Rumaila, make up Rumaila Field, a gently sloping longitudinal anticline structure (Chafeet and Handhal, 2023). The North Rumaila dome is an elongated, asymmetric anticline with a predominantly north-south orientation (Handhal et al., 2019). Its flanks exhibit a gentle dip of approximately 3 degrees, with the western flank slightly steeper than the eastern side (Ismail et al., 2021). The dome gently plunges southward to form a saddle that separates it from the South Rumaila dome (Handhal et al., 2019).

Stratigraphically, the Zubair Formation consists of 380–400 meters of shale, siltstone, and sandstone alternating with each other (Al-Jaberi and A-Jafar, 2020).The Arabian Plate categorizes the Cretaceous succession into two megasequences, AP8 and AP9. This framework classifies the Zubair Formation, under the AP8 megasequence making it the fourth super-sequence in the upper portion of the Thammama Group (Watson and Chang, 1997). The Aptian Shuaiba Formation conformably and gradationally overlies the Zubair Formation, which in turn conformably underlies the shales and limestones of the Valanginian-Hauterivian Ratawi Formation (Watson and Chang, 1997). The Zubair Formation in southern Iraq is divided into informal members, listed from oldest to youngest: the lower shale member (Z/6), the lower sand member (4th Pay, Z/5), the middle shale member (Z/4), the upper sand member (Z/2A), and the upper shale member as shown in Fig. 2. (Wells et al., 2017). The Upper Sand Member, also referred to as the "main pay," comprises five primary units. Three of these are sandstone units that serve as reservoir units (AB, DJ, LN), while the remaining two are shale units (C, K) acting as barriers to vertical fluid movement within the reservoir (Fig. 2) (Mohammed et al., 2010).

The Upper Sandstone Member was formed in a tidal or estuarine environment, characterized by the widespread deposition of sand channels throughout the formation (Al-Aradi et al., 2022). Al-Jaberi and Al-Mayyahi (2018) demonstrated that the porosity and permeability of the Zubair Formation in the southern part of Rumaila are superior to those in the northern part. This difference is attributed to the sand grains in the northern Rumaila being coated with silt grains, which negatively impacts their porosity and permeability. Al-Aradi et al. (2022) conducted a study on the Zubair Formation in the Rumaila oilfield using open-hole logs from eight wells. The results revealed high porosity (ranging from 15% to

25%), good to excellent permeability, and significant hydrocarbon productivity. These characteristics were attributed to high oil saturation, good effective porosity, and low shale volume, with net pay thicknesses ranging from 5 to 59 meters. Al-Samer and Al-Najm (2024) conducted an examination of the petrophysical characteristics of the Upper Sand Member (Main Pay) of the Zubair Formation using data from four wells in the South Rumaila oilfield. Through statistical analysis, they revealed that the reservoirs are heterogeneous and can be classified into four facies: Sand, Shaly Sand, Sandy Shale, and Shale. The findings indicate favorable petrophysical characteristics for the reservoir.

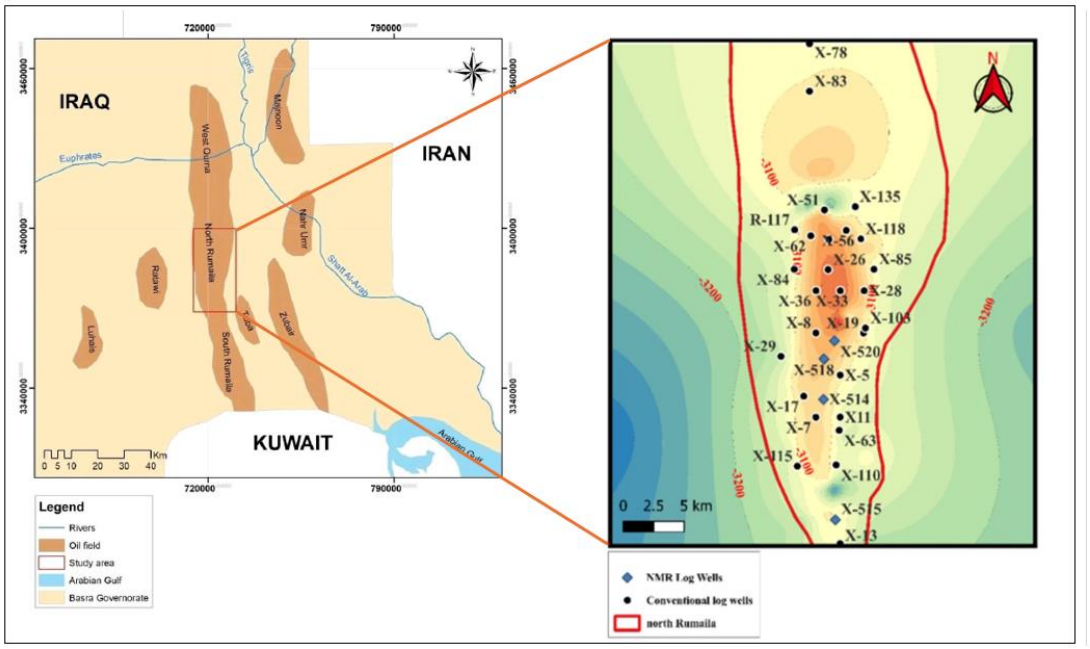

Fig.1. Structural map of the North Rumaila oil field with selected wells for this study

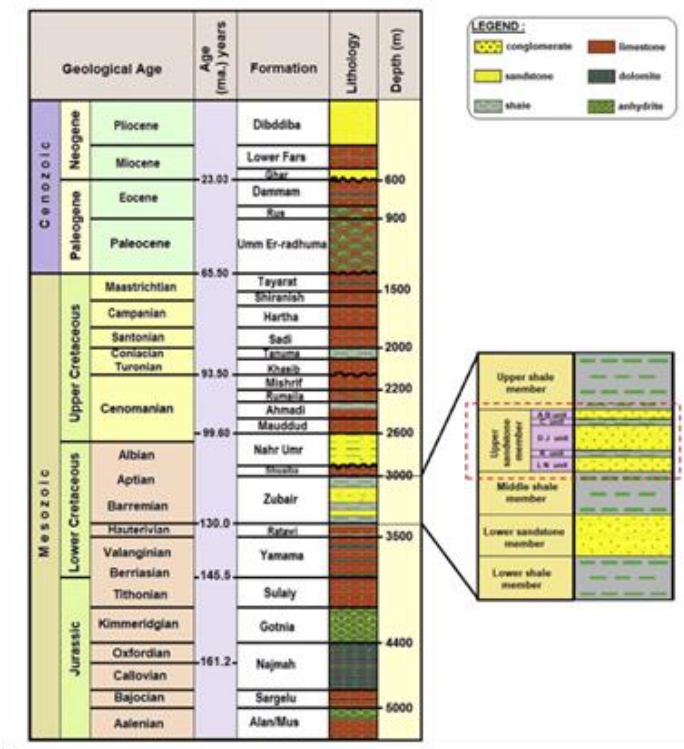

Fig. 2. Stratigraphical column at Rumaila oilfield after Handhal et al. (2020)

3. Materials and Methods

The research employed Techlog 2018, a sophisticated well log interpretation software developed by Schlumberger. A comprehensive set of open-hole logs was utilized to determine the petrophysical characteristics of the Zubair Formation. The logs used in this analysis include:

3.1. Well Logs Utilized in This Study

3.1.1. Caliper log

A caliper toll is employed to precisely determine the shape and diameter of a borehole at different depths (Paske et al., 1990). The caliper log indicates locations where the well diameter has expanded due to breakouts, washouts, or cavity formation. It also identifies areas where the well diameter has narrowed due to the creating a mud cake compared to the permeable sections (Elahifar et al., 2012).

3.1.2. Gamma Ray Log (GR)

The gamma-ray log measures the natural radioactivity present in geological formations. It is particularly effective at differentiating between shaly and clean formations. Shales typically exhibit high gamma-ray readings, whereas sandstones and carbonates show lower readings (Stick Jr and Hartline, 1962). Gamma-ray log analysis revealed elevated readings in the C and K layers, indicating shale-rich lithology, whereas lower readings in the AB, DJ, and LN layers suggest cleaner sandstone, potentially representing reservoir zones.

3.1.3. Neutron Log (NPHI)

A neutron log, a well logging tool, quantifies the hydrogen concentration in geological formations, a process often linked to the formation's porosity. By sending neutrons into the formation and detecting the slowed-down neutrons that return, it provides indirect information on the presence of fluids especially oil, gas, and water (Liu, 2017).

3.1.4. Density Log (RHOB)

A density log, a well-logging tool, measures the bulk density of geological formations. By emitting gamma rays into the formation and detecting the extent of radiation absorption, it provides valuable insights into the rock's porosity and lithology. When combined with the neutron log, it enables more accurate porosity measurements (Horsfall et al., 2013).

In this context, the neutron and density logs (NPHI, RHOB) exhibit distinct separation patterns. A positive separation, indicating an increase in both neutron porosity and density, is observed in the presence of dirty or shale rocks, as seen in the C and K units. Conversely, a negative separation is recorded for sandy rocks, where the neutron log shows lower porosity values, as observed in the AB, DJ, and LN layers.

3.1.5. Sonic Log (DT)

The sonic log is classified as a porosity log because it estimates primary porosity, specifically matrix porosity, while excluding vuggy porosity and fractures. This device measures the travel time of the acoustic wave through one foot of the formation, expressed in microseconds per foot or microseconds per meter and it exhibits an inverse relationship with velocity (Liu, 2017).

3.1.6. Resistivity Logs

The resistivity log quantifies the formation's capacity to impede the movement of electric current, providing insights into the rock's composition and fluid content (Archie, 1942). Water typically demonstrates low resistivity, indicating its high conductivity. In contrast, hydrocarbons display higher resistivity values relative to water, reflecting their lower electrical conductivity (Doveton and Prensky, 1992). In this context, the resistivity log exhibited high readings in the AB and DJ layers, suggesting the potential presence of high hydrocarbon saturation values. In contrast, the LN layer showed fluctuating readings, which may indicate variability in hydrocarbon distribution or differences in reservoir quality.

3.1.7. Nuclear Magnetic Resonance (NMR)

A nuclear magnetic resonance log is a geophysical investigation technique that entails examining underground formations and obtaining data about their characteristics. NMR tools provide mineralogy-independent measurements of porosity (direct porosity), accurately measuring the quantity of fluid in the pore space without considering the rock matrix (Mitchell et al., 2013). Unlike other porosity devices, NMR tools do not require information about the matrix or fluid density to compute porosity (Watson and Chang, 1997). The NMR service largely relies on detecting hydrogen protons located inside the formation's pores, facilitating porosity measurement. NMR porosity, in contrast to adjusted neutron porosity, neglects hydrogen that is firmly bonded within the rock matrix, thereby offering an independent porosity measurement of lithology (Liu, 2017).

3.2. Volume of Shale Calculation

There are several methods used to calculate shale volume, and the method applied in this study relies on the gamma-ray log, which is the most effective tool for this purpose. It uses the following equation:(Szabó, 2011).

$$V_{sh} = 0.33\left(2^{(2*IGR)} - 1\right) \quad \text{.....} \quad (1)$$

However, before calculating the shale volume(V_{sh}), it is essential first to determine the gamma-ray index (IGR).

$$\mathrm{IGR} = \frac{\mathrm{GR\,log} - \mathrm{GR\,min}}{\mathrm{GR\,max} - \mathrm{GR\,min}} \quad \text{.....} \quad (2)$$

Where: IGR = gamma-ray index. GR log = gamma-ray of formation. GR max = gamma-ray of shale. GR min = gamma-ray of clean formation

Depending on the Vsh values derived from (equation 1) for each well, the clean zones (Sand) were identified as having a Vsh value of less than 10%, while the unclean zones (Dirty and Shale) were identified as having a Vsh value of 10% or higher.

3.3. Porosity Calculation

To determine porosity, the following logs were utilized:

3.3.1. Sonic porosity

The sonic log was employed to calculate the primary porosity, based on the following equation: (Wyllie et al., 1958).

$$\emptyset_s = \frac{\Delta\mathrm{tlog} - \Delta\mathrm{tma}}{\Delta\mathrm{tfl} - \Delta\mathrm{tma}} \quad \text{.....(3)}$$

The alternate equation suggested by Atlas was utilized for the dirty zones characterized by a Vsh greater than 10% (Kamel and Mohamed, 2006).

$$\varnothing_{\mathrm{sc}} = \left(\frac{\Delta \mathrm{t\,log} - \Delta \mathrm{tma}}{\Delta \mathrm{tfl} - \Delta \mathrm{tma}}\right) - \left(\frac{\Delta \mathrm{tsh} - \Delta \mathrm{tma}}{\Delta \mathrm{tfl} - \Delta \mathrm{tma}a}\right) * Vsh \quad \ldots\ldots\ldots\ldots\ldots\ldots(4)$$

Where: Øs = sonic-derived porosity. Δt log = the interval transit time in the formation measured by the log (μs/ft). Øsc = Sonic porosity adjusted for shale content. Δt ma = the interval transit time in the rock matrix. Δt f = the interval transit time in the formation (189). Δt sh = the interval transit time in nearby shale.

3.3.2. Density porosity

The Wyllie equation (Wyllie et al., 1958) was employed to determine the porosity of the formation in clean zones (Vsh < %10) using the density tool.

$$\varnothing_{\mathrm{D}} = \frac{\rho \mathrm{ma} - \rho\ \mathrm{bulk}}{\rho \mathrm{ma} - \rho \mathrm{f}} \quad \ldots\ldots\ldots\ldots\ldots \quad (5)$$

Where: $\varnothing_{\mathrm{D}}$ = density-derived porosity.ρ ma = density of formation. ρ bulk = density log reading. ρfl = density of fluid.

The Dresser Atlas equation was applied to zones where the shale volume exceeds 10% (Kamel and Mabrouk, 2003).

$$\varnothing_{\mathrm{DC}} = \left(\frac{\rho \mathrm{ma} - \rho\ \mathrm{bulk}}{\rho \mathrm{ma} - \rho \mathrm{fl}}\right) - \left(\frac{(\rho \mathrm{ma} - \rho \mathrm{sh}}{\rho \mathrm{ma} - \rho \mathrm{fl}}\right) * Vsh \quad \ldots\ldots\ldots\ldots(6)$$

Where: D Corr = corrected density porosity, ρsh = density of shale

3.3.3. Neutron porosity

If the shale content in the reservoir exceeds 10% , the neutron porosity values need to be adjusted using the following calculation (Kamel and Mabrouk, 2003).

$$\Phi_{\mathrm{N\ corr}} = \phi_{\mathrm{N\,log}} - \left(\phi_{\mathrm{n\ sh}} * \mathrm{V_{sh)}}\right) \quad \ldots\ldots\ldots \quad (7)$$

Where:$\phi_{\mathrm{N\ corr}}$ = correct neutron porosity. $\phi_{\mathrm{N\ log}}$ = neutron porosity from log. Nsh = neutron porosity for shale.

To calculate the total porosity and effective porosity, the following equation was used:

Total porosity $\Phi_{\mathrm{t}} = \frac{\Phi \mathrm{D} + \Phi \mathrm{N}}{2}$ …….. (8)

Where: $\varnothing_{\mathrm{N.D}}$ = Total porosity is determined by utilizing density and neutron tools.

effective porosity $(\phi_e) = [(\phi_{\mathrm{Dcorr}} + \phi_{\mathrm{Ncorr}})/2] \times (1 - \mathrm{V_{sh}})$ …….. (9)

The secondary porosity was determined for depth intervals with shale content below 10% using the specified equation (Abdul-majeed et al., 2020)

$$\mathrm{SPI} = \emptyset_{\mathrm{N.D}} - \emptyset_{\mathrm{S}} \quad \ldots\ldots\ldots\ldots \quad (10)$$

The alternative equation was applied to zones where the shale volume exceeded 10%.

$$\mathbf{SPI}_{\mathrm{c}} = \emptyset_{\mathrm{N.Dc}} - \emptyset_{\mathrm{Sc}} \quad (11)$$

3.4. Fluid Saturation Calculation

To calculate the water saturation for the invaded zone and the uninvaded zone of a formation with a shale volume of less than 10%, the Archie's equation for clean formations were used:

$$S_W = \sqrt{\frac{F * RW}{RT}} \quad \ldots\ldots\ldots\ldots \quad (12)$$

Where: S_W = water saturation. Rw = the resistivity of formation water.Rt = true resistivity recorded by log (Ωm)).F = Formation factor.

$$S_{XO} = \sqrt{\frac{F * Rmf}{RT}} \quad \ldots\ldots\ldots\ldots\ldots \quad (13)$$

Where:

S_{xo} = water saturation of the invaded zone. R_{mf} = the resistivity of the mud filtrate at the temperature of the formation. R_{xo} = invaded zone Resistivity.

The calculation of Sw for shale volumes (Vsh) above 10% or 15% was performed using the equation of (Simandoux, 1963).

$$S_W = \left[\frac{0.4 * Rw}{\phi^2}\right] * \left[\sqrt{\left\{\left(\frac{Vsh}{Rsh}\right)^2 + \left(\frac{5 * \emptyset^2}{Rt * Rw}\right)\right\}} - \left(\frac{Vsh}{Rsh}\right)\right] \quad \ldots\ldots\ldots\ldots\ldots \quad (14)$$

Where Sw = water saturation of the uninvaded zone. Rsh = true resistivity of nearby shale.Rt = true resistivity of uninvaded zone.

The hydrocarbon saturation (Sh) is computed using the following equation:

$$S_h = 1 - S_w \quad \ldots\ldots\ldots\ldots \quad (15)$$

3.5. Estimation of Bulk Water Volume and Movable Hydrocarbon

To compute bulk water volume (BVW) and bulk volume hydrocarbon (BVH), the following equations were used

$$BV_W = S_W * \emptyset_{N.D} \quad \ldots\ldots\ldots\ldots \quad (16)$$

$$BV_h = S_h * \emptyset_{N.D} \quad \ldots\ldots\ldots\ldots \quad (17)$$

In addition, it computes the movable oil saturation (MOS) using the specified equation (Spain, 1992):

$$MOS = S_{XO} - S_W \quad \ldots\ldots\ldots\ldots \quad (18)$$

The residual oil saturation can be computed using the following equation:

$$ROS = 1 - S_{XO} \quad \ldots\ldots\ldots\ldots \quad (20)$$

3.6. Permeability Calculation (K_{NMR})

There are several models available for calculating permeability using NMR logging tools; however, this study selected the Mean T2 (SDR) permeability model. This method estimates permeability based on NMR porosity and the duration of T2 relaxation time in the formation. The equation used is as follows:

$$K_{NMR} = C(\Phi_{NMR})^4 (T_{2LM})^2 \quad \ldots.(21)$$

Where: Φ is the effective porosity from NMR, T_{2LM} is the geometric mean of the T2 relaxation time,and C is a lithology-dependent variable. In sandstone, C is equal to 4, while in carbonate, C is equal to 0.1

4. Results and Discussion

4.1. Conventioal log Result

We have identified three permeable layers (AB, DJ, and LN) and two impermeable units (C and K) based on the behavior of the well logs, such as the Gamma Ray (GR) log, resistivity logs and porosity logs like RHOB, NPHI, and DT at the layer boundaries, as shown in Fig. 6. The following is a description of the key petrophysical properties of these reservoir units based on the analysis of well logs from the study area.

4.1.1. Unit AB

The AB unit, a key reservoir unit within the Upper Zubair Member is characterized by its distinct reservoir properties. The area's lithology primarily consists of sandstone with interspersed shale. Al-Aradi et al. (2022) indicate that a sandstone layer, progressively transitioning from the USM layer borders the AB layer above, while the impermeable C layer consisting of shale forms its lower boundary. The AB layer is the thinnest among the main pay permeable layers, with thicknesses ranging from 2.74 meters in well X-75 to 11.3 meters in well X-5, as shown in Fig. 3A. Petrophysical analysis revealed variations in shale volume among the study wells, with well X-63 exhibiting the lowest shale content. Additionally, Fig. 3B depicts the spatial distribution of shale volume within the AB layer, where a notable northward increase in shale content is observed. Effective porosity values also varied across the study wells. Wells X-85, X-83, X-7and X-67 demonstrated very good porosity, whereas wells X-56 and X-016 displayed fair porosity as shown in Fig. 3C. The remaining wells showed good porosity values. Furthermore, Fig. 3D illustrates the spatial distribution of hydrocarbon saturation values, which were high in all wells. When comparing this unit across all wells, well X-5 stands out as the best due to its greater thickness and advantageous reservoir characteristics, as highlighted in Table **1**.

Table 1. Illustration of the thickness and depth of the reservoir unit (AB) and the Petrophysical results in the Study wells

Well NO.	Depth (m)	Thickness (m)	Average (%)			
			Vsh	PHIT	PHIE	S_h
X-5	3178.90-3190.20	11.3	0.08	0.21	0.19	0.88
X-7	3161.51-3167.69	6.18	0.10	0.23	0.21	0.77
X-8	3119.80-3126.50	6.7	0.11	0.22	0.19	0.82
X-11	3219.90-3227.52	7.62	0.15	0.19	0.16	0.82
X-13	3204.00-3208.72	4.72	0.12	0.14	0.12	0.70
X-17	3201.77-3209.84	8.07	0.12	0.18	0.16	0.78
X-19	3211.85-3217.03	5.18	0.12	0.16	0.14	0.69
X-26	3087.53-3090.38	2.85	0.22	0.19	0.15	0.69
X-28	3159.80-3169.70	9.91	0.26	0.24	0.18	0.75
X-29	3253.15-3253.15	6.70	0.10	0.18	0.16	0.70
X-33	3253.80-3259.87	6.07	0.13	0.22	0.19	0.79
X-36	3117.17-3124.00	6.83	0.07	0.19	0.18	0.78
X-51	3121.09-3125.62	4.53	0.18	0.18	0.15	0.66

X-56	3137.6-3141.68	4.08	0.25	0.17	0.13	0.62
X-62	3137.95-3142.22	4.26	0.20	0.26	0.21	0.67
X-63	3226.61-3233.77	7.16	0.05	0.17	0.16	0.71
X-68	3103.85-3107.20	3.35	0.20	0.22	0.18	0.60
X-78	3213.80-3216.54	2.74	0.34	0.22	0.14	0.53
X-83	3201.27-3207.94	6.67	0.20	0.29	0.23	0.68
X-84	3219.18-3225.54	6.36	0.12	0.18	0.16	0.77
X-85	3212.44-3220.85	8.41	0.23	0.31	0.24	0.75
X-103	3206.02-3212.88	6.86	0.11	0.19	0.16	0.78
X-110	3212.60-3221.50	8.9	0.06	0.18	0.17	0.88
X-115	3205.90-3216.50	10.6	0.09	0.21	0.19	0.84
X-117	3200.81-3204.72	5.15	0.16	0.24	0.19	0.72
X-118	3184.19-3188.50	4.31	0.21	0.23	0.18	0.64
X-135	3199.18-3203.90	4.72	0.30	0.24	0.16	0.62

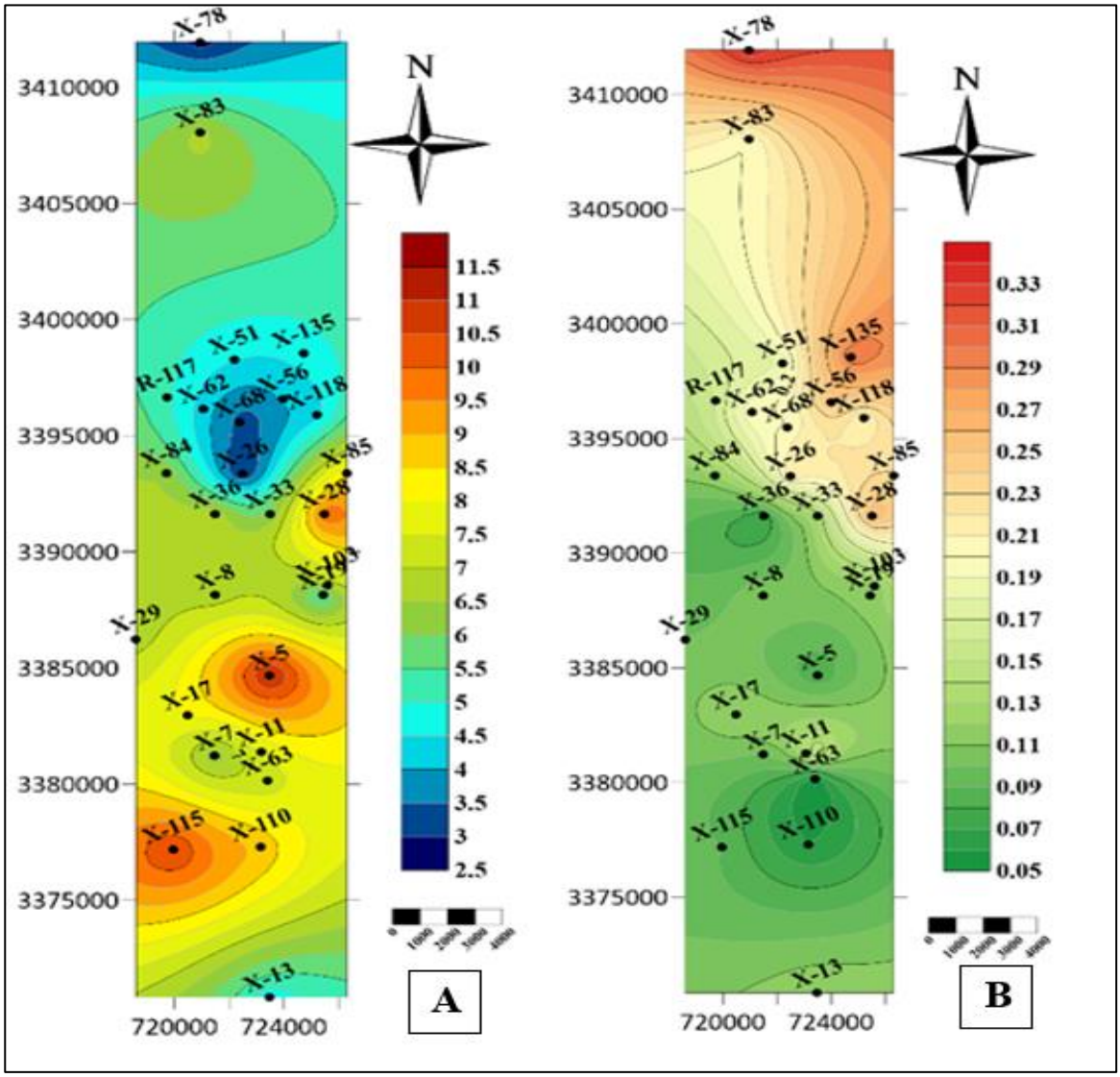

Fig. 3. Maps Shown the spatial distribution of (A) thickness, and (B) shale volume for the AB layer of Zubair Formation in the North Rumaila field

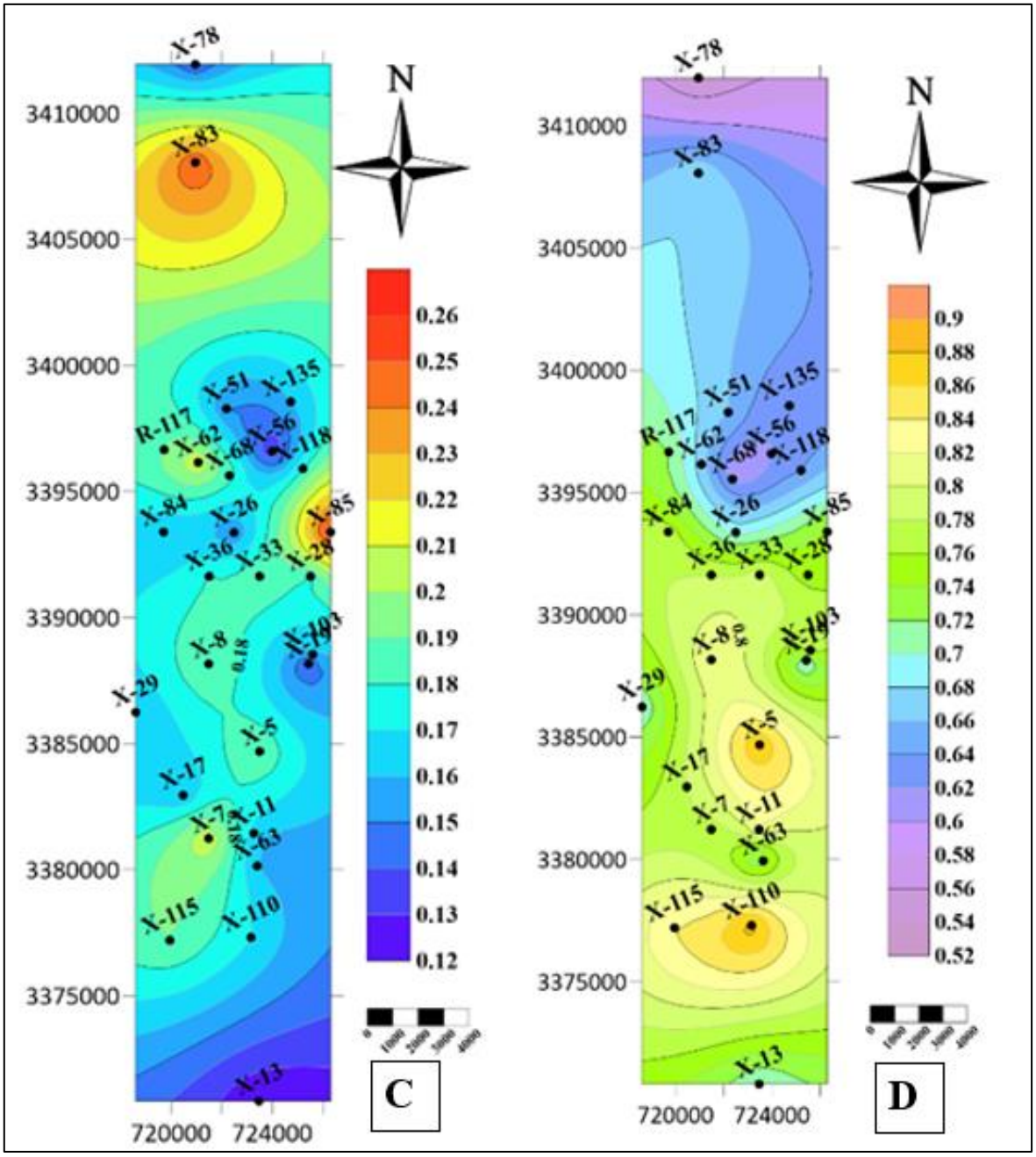

Fig.4. Maps Shown the spatial distribution of (C) porosity, and (D) hydrocarbon saturation for the AB layer of Zubair Formation in the North Rumaila field

4.1.2. Unit C

An impermeable layer composed of shale separates the AB reservoir unit above from the DJ reservoir unit below, with a thickness ranging from 4.4 to 10.05 meters in the studied wells.

4.1.3. Unit DJ

This uint, primarily composed of sandstone with thin interlayers of shaly sand, has been subdivided into secondary units.The thickness of this layer, which ranges from 45.1 meters in well X-11 to 64.22 meters in well X-85, is considered the thickest among the three permeable uints, as illustrated in Fig. 4A. Two impermeable units confine unit DJ: it is overlain by the C uint and underlain by the K unit, which consists of shale. The petrophysical properties revealed good effective porosity values across all

study wells, with the exception of wells X-103, X-78, X-29, X-135, X-68, X-62, and X-56 where the values were deemed fair, as shown in Fig. 4C. On the other hand, the shale volume values were high in all study wells within this layer, with the exception of wells X-63 and X-115. Fig. 4B illustrates the spatial distribution of shale volume within the DJ layer, revealing a significant increase in shale content toward the north. This trend can be attributed to the marine regression that occurred from the southern part of the field towards the north. Areas exposed during the marine regression exhibit lower clay content, while regions that remained submerged exhibited relatively higher shale content due to prolonged marine influence. In contrast, hydrocarbon saturation levels were found to be high across all study wells, with the exception of well X-78, as shown in Table 2 and Fig. 4D. Among all study wells, well X-8 exhibits the most favorable petrophysical properties. Conversely, well X-78 demonstrates the least favorable properties compared to the other wells.

Table 2. Demonstrate the thickness, depth of the reservoir unit (DJ) and the Petrophysical results in the Study wells

WELL NO	Depth (m)	Thickness (m)	Average (%)			
			Vsh	PHIT	PHIE	S_h
X-5	3194.50-3253.90	59.4	0.18	0.20	0.17	0.75
X-7	3174.58-3231.12	56.54	0.12	0.20	0.18	0.87
X-8	3132.90-3193.80	60.9	0.11	0.23	0.20	0.87
X-11	3233.01-3278.32	45.1	0.18	0.20	0.16	0.82
X-13	3217.86-3269.99	52.1	0.13	0.19	0.17	0.80
X-17	3213.50-3258.61	45.1	0.18	0.20	0.17	0.82
X-19	3278.60-3278.60	53.34	0.18	0.18	0.15	0.71
X-26	3100.43-3150.35	49.92	0.17	0.21	0.17	0.77
X-28	3178.85-3229.75	50.9	0.22	0.19	0.15	0.82
X-29	3268.39-3321.12	52.73	0.14	0.15	0.13	0.65
X-33	3088.50-3144.30	55.8	0.22	0.20	0.15	0.74
X-36	3130.84-3187.68	56.84	0.18	0.19	0.15	0.72
X-51	3131.80-3186.94	55.14	0.21	0.23	0.17	0.77
X-56	3148.82-3194.77	45.95	0.28	0.19	0.14	0.72
X-62	3150.75-3203.789	53.03	0.24	0.19	0.14	0.72
X-63	3240.31-3296.00	55.69	0.09	0.16	0.15	0.83
X-68	3115.13-3161.00	45.87	0.25	0.19	0.14	0.64
X-78	3223.09-3269.88	46.79	0.40	0.23	0.13	0.56
X-83	3212.59-3263.02	50.43	0.28	0.27	0.19	0.67
X-84	3229.95-3284.57	54.62	0.17	0.19	0.15	0.74
X-85	3225.87-3290.09	64.22	0.23	0.20	0.15	0.80
X-103	3220.01-3271.79	51.78	0.29	0.21	0.13	0.77
X110	3227.40-3282.00	54.6	0.14	0.19	0.17	0.85
X-115	3221.97-3279.45	57.48	0.09	0.19	0.17	0.87
X-117	3209.87-3267.00	57.13	0.16	0.21	0.17	0.84
X-118	3194.94-3254.00	59.06	0.20	0.18	0.15	0.78
X-135	3210.76-3265.62	54.86	0.33	0.24	0.14	0.71

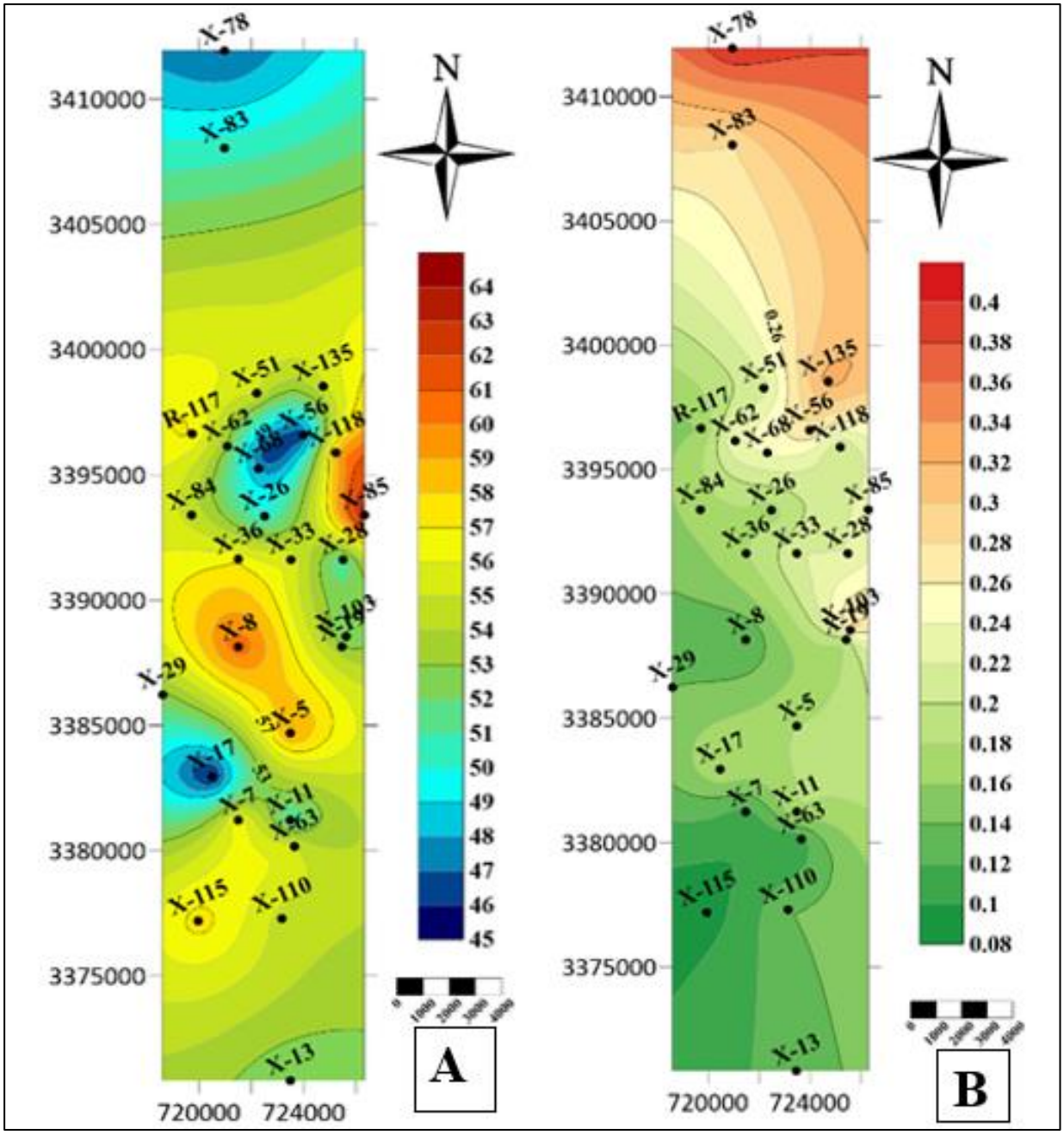

Fig. 5. Maps showing the spatial distribution of (A) thickness, and (B) shale volume for the DJ layer of Zubair Formation in the North Rumaila field

4.1.4. Unit K

An impermeable layer composed of shale separates the DJ reservoir unit above from the LN reservoir unit below, with a thickness ranging from 2.39 to 8.98 meters in the study wells.

4.1.5. Unit LN

The thickness of this unit ranges from 18.75 meters in well X-19 to 48.01 meters in well X-83, as shown in Fig. 4A. However, data for wells X-5, X-11, X-17, and X-29 are incomplete due to missing records, as highlighted in Table 3. Furthermore, shale volume is distributed throughout the entire unit across all wells, with an increase observed near its termination (the beginning of the Middle Shale Member). Additionally, shale volume is relatively low in wells X-115, X-7, X-13, X-56, and X-62. In

contrast, the remaining wells exhibited a noticeable increase in shale volume values, as shown in Fig. 5B. Moreover, effective porosity values ranged from fair, as observed in wells X-118, X-26, X-36, X-51, X-063, X-68, X-19, X-28, X-84, and X-85, to good in the remaining study wells, as shown in Fig. 4C. Low hydrocarbon saturation values were found in wells X-115, X-19, X-84, X-110, X-63, X-78, X-13, X-103, and X-85, while the remaining wells demonstrated elevated saturation values, as shown in Fig. 4D.

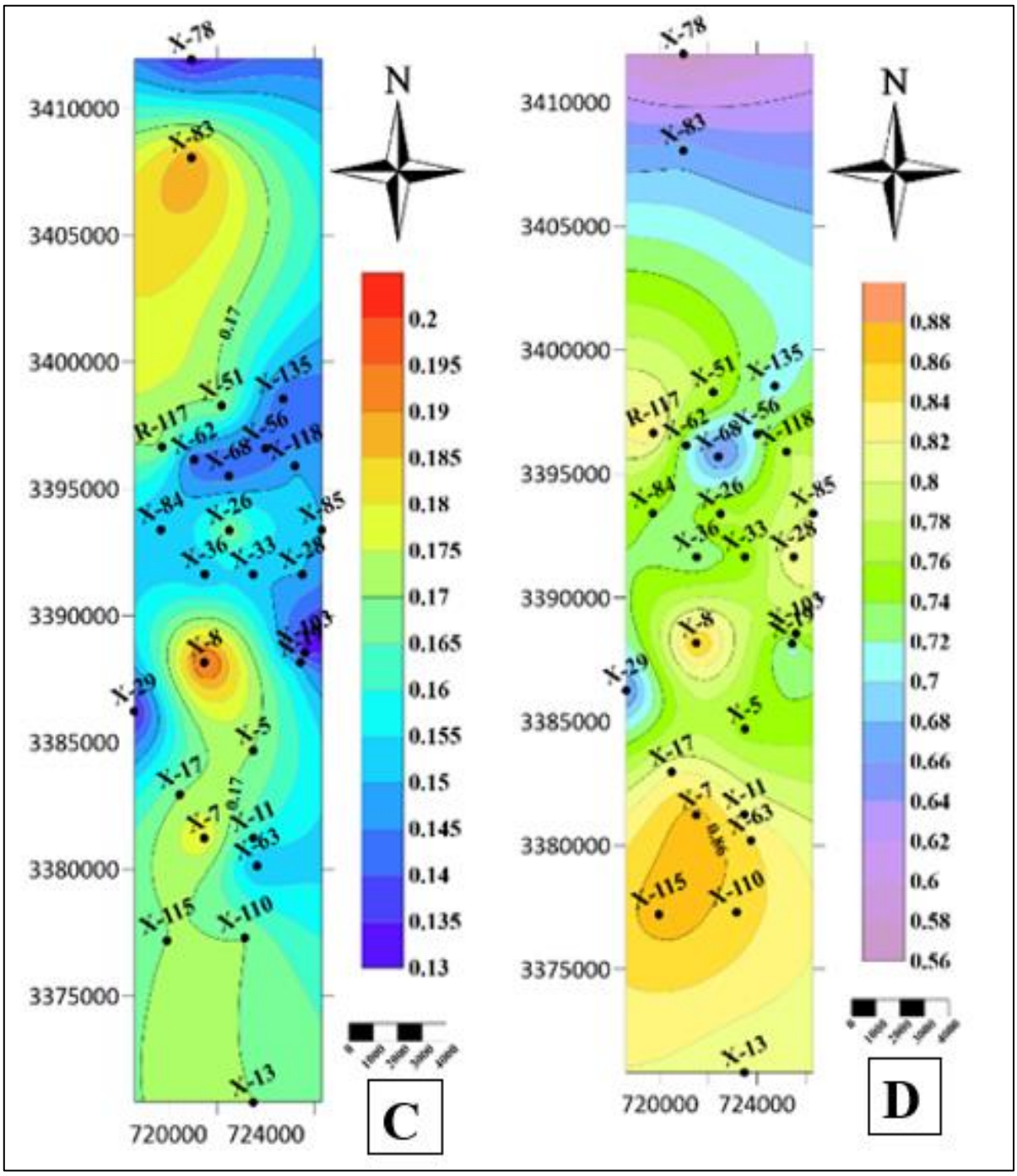

Fig. 6. Maps showing the spatial distribution of (C) porosity, and (D) hydrocarbon saturation for the DJ layer of Zubair Formation in the North Rumaila field

Table 3. Illustrate the thickness and depth of the reservoir unit (LN) and the Petrophysical results in the Study wells

WELL NO	Depth (m)	Thickness (m)	Average (%)			
			Vsh	PHIT	PHIE	S_h
X-5	-	-	-	-	-	-
X-7	3235.39-3271.5	36.11	0.08	0.20	0.18	0.84
X-8	3197.5-3239.3	41.8	0.12	0.21	0.18	0.85
X-11	-	-	-	-	-	-
X-13	3276.23-3317.84	41.6	0.09	0.17	0.15	0.38
X-17	-	-	-	-	-	-
X-19	3287.44-3306.19	18.75	0.19	0.18	0.14	0.22
X-26	3153.56 -3184.92	31.36	0.25	0.16	0.12	0.70
X-28	3278.21-3236.61	41.6	0.21	0.18	0.14	0.80
X-29	-	-	-	-	-	-
X-33	3149.09-3185.57	36.48	0.22	0.19	0.15	0.77
X-36	3192.65-3226.01	33.36	0.12	0.15	0.13	0.74
X-51	3191.24-3225.71	34.47	0.29	0.20	0.13	0.68
X-56	3203.75-3235.70	31.95	0.09	0.18	0.17	0.80
X-62	3207.59-3244.48	36.88	0.09	0.21	0.20	0.70
X-63	3301.20-3332.77	31.57	0.15	0.15	0.13	0.24
X-68	3169.68-3209.31	39.62	0.17	0.16	0.13	0.66
X-78	3279.63-3313.47	33.83	0.20	0.20	0.16	0.31
X-83	3266.73-3300.08	33.35	0.22	0.23	0.17	0.53
X-84	3287.50-3335.51	48.01	0.13	0.16	0.14	0.22
X-85	3294.66-3331.02	36.36	0.18	0.18	0.14	0.40
X-103	3277.04-3313.73	36.69	0.21	0.18	0.14	0.39
X-110	3286.50-3322.97	36.47	0.11	0.18	0.16	0.23
X-115	3283.20-3319.19	35.99	0.07	0.18	0.17	0.15
X-117	3273.25-3308.51	35.26	0.18	0.21	0.16	0.40
X-118	3260.53-3298.99	38.46	0.42	0.18	0.10	0.66
X-135	3271.72-3307.99	36.27	0.26	0.20	0.14	0.55

4.2. NMR LOG Discussion

Based on the NMR findings, the AB layer exhibited effective porosity values ranging from good to fair, with permeability values varying from very good to excellent, particularly in well X-515. In contrast, the DJ layer demonstrated good effective porosity across all wells, except for well X-520, and consistently showed very good permeability values, except for well X-514. The LN layer, however, displayed fair effective porosity throughout all wells, while permeability was generally classified as very good, except in well X-514, where it was rated as good, as shown in Tables 4 and Fig. 7.

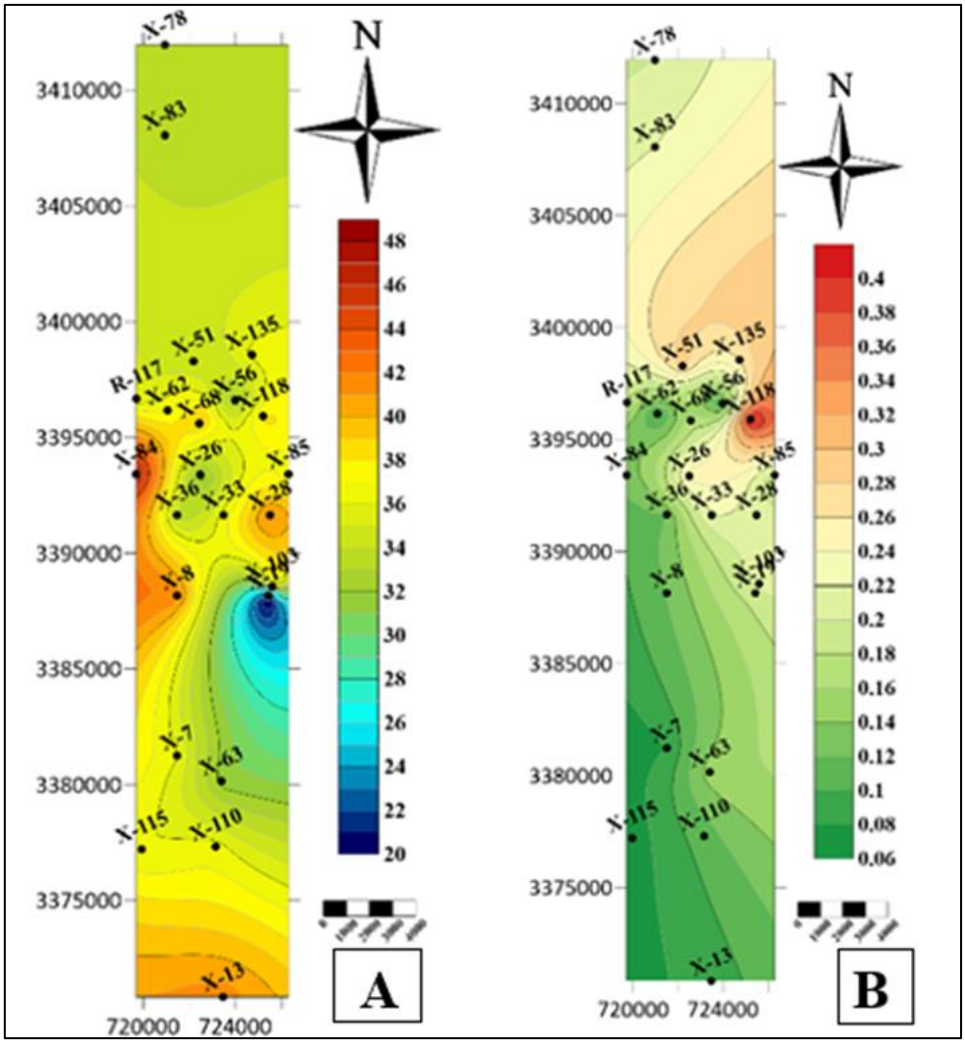

Fig.7. Maps showing the spatial distribution of (A) thickness, and (B) shale volume for the LN layer of Zubair **F**ormation in the North Rumaila field

5. Conclusions

The Upper Sand Member of the Zubair Formation is divided into three permeable layers (AB, DJ, and LN) and two impermeable layers. There is a notable northward increase in shale content across the field, likely shaped by the depositional environment of the North Rumaila Field. This trend can be attributed to a marine regression progressing from the southern to the northern part of the field, As a result, areas that were exposed experienced reduced clay content due to coarser sediment deposition, while submerged regions experienced prolonged marine influence, leading to finer sediment accumulation and higher shale content. Log analysis reveals that the AB layer, despite its limited thickness, exhibits the lowest shale content, good porosity, high hydrocarbon saturation, and very good permeability, making it the most favorable reservoir. Conversely, the LN layer has the least favorable characteristics, with higher shale content, lower porosity, and reduced hydrocarbon saturation and permeability. The DJ unit demonstrates generally good reservoir properties, with moderate shale content, good porosity, high hydrocarbon saturation, and the greatest thickness among all layers. These findings highlight the importance of understanding the geological features of the Zubair Formation for optimized reservoir management and exploration strategies. Development wells should focus on the AB and DJ layers in the southern and central parts of the field, where favorable reservoir properties are concentrated.

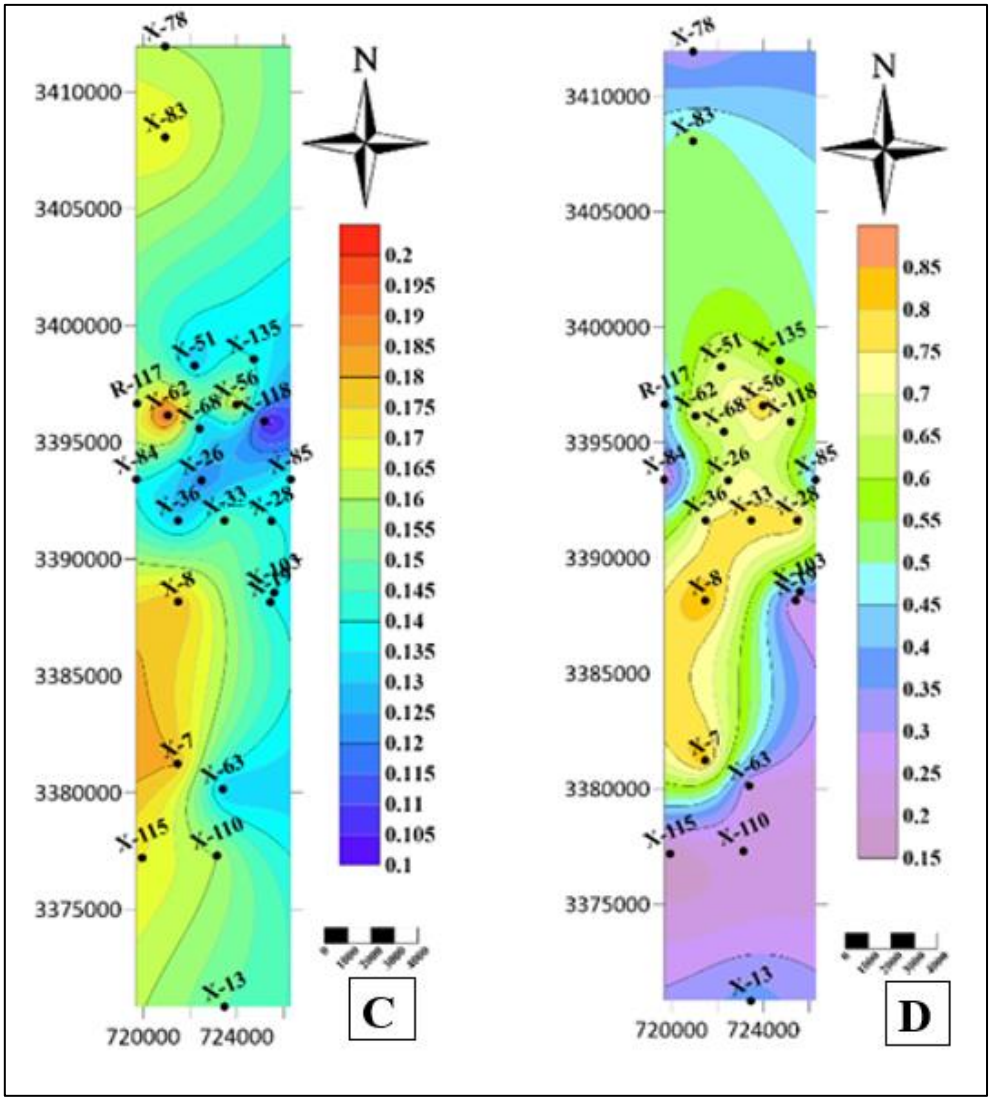

Fig.8. Maps showing the spatial distribution of (C) porosity and (D) hydrocarbon saturation for the LN layer of Zubair **F**ormation in the North Rumaila field

Table 4. NMR Log Results for the AB Unit

WELL NO	Uint	Depth (m)	Thickness (m)	Average (%)		
				T2 PHIT	T2 PHIE	KSDR
R-514	AB	3143.15-3152.95	9.8	0.19	0.16	77.72
	DJ	3210.95-3159.15	51.8	0.13	0.11	89.3
	LN	3214.15-3256.55	42.4	0.14	0.13	71.07
R-515	AB	3206.323212.32	0.19	0.18	0.19	196.53
	DJ	3217.32-3278.32	61.0	0.17	0.14	537.77
	LN	3284.32-3320.32	36.0	0.24	0.14	165.35
R-518	AB	3152.79-3159.95	7.16	0.17	0.13	198.09
	DJ	3165.13-3222.89	57.76	0.15	0.13	831.24
	LN	3226.09-3262.67	36.58	0.14	0.12	644.21
R-520	AB	3133.6-3140.92	7.32	0.18	0.15	519.88
	DJ	3146.10-3202.94	56.84	0.17	0.15	910.91
	LN	3207.06-3246.38	39.32	0.15	0.12	752.50

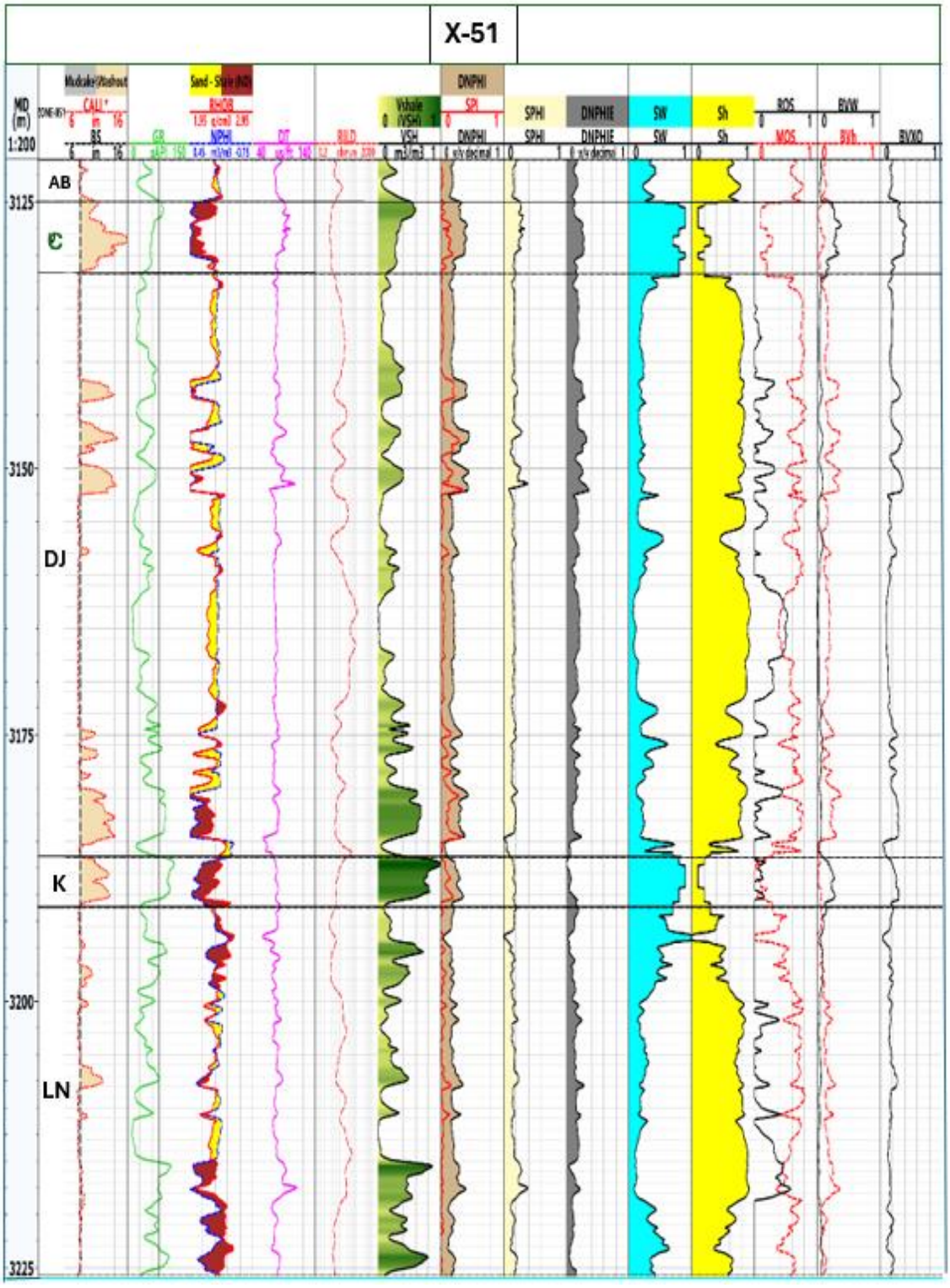

Fig.9. Open-hole logs and CPI of the Zubair Formation in North Rumaila oilfield

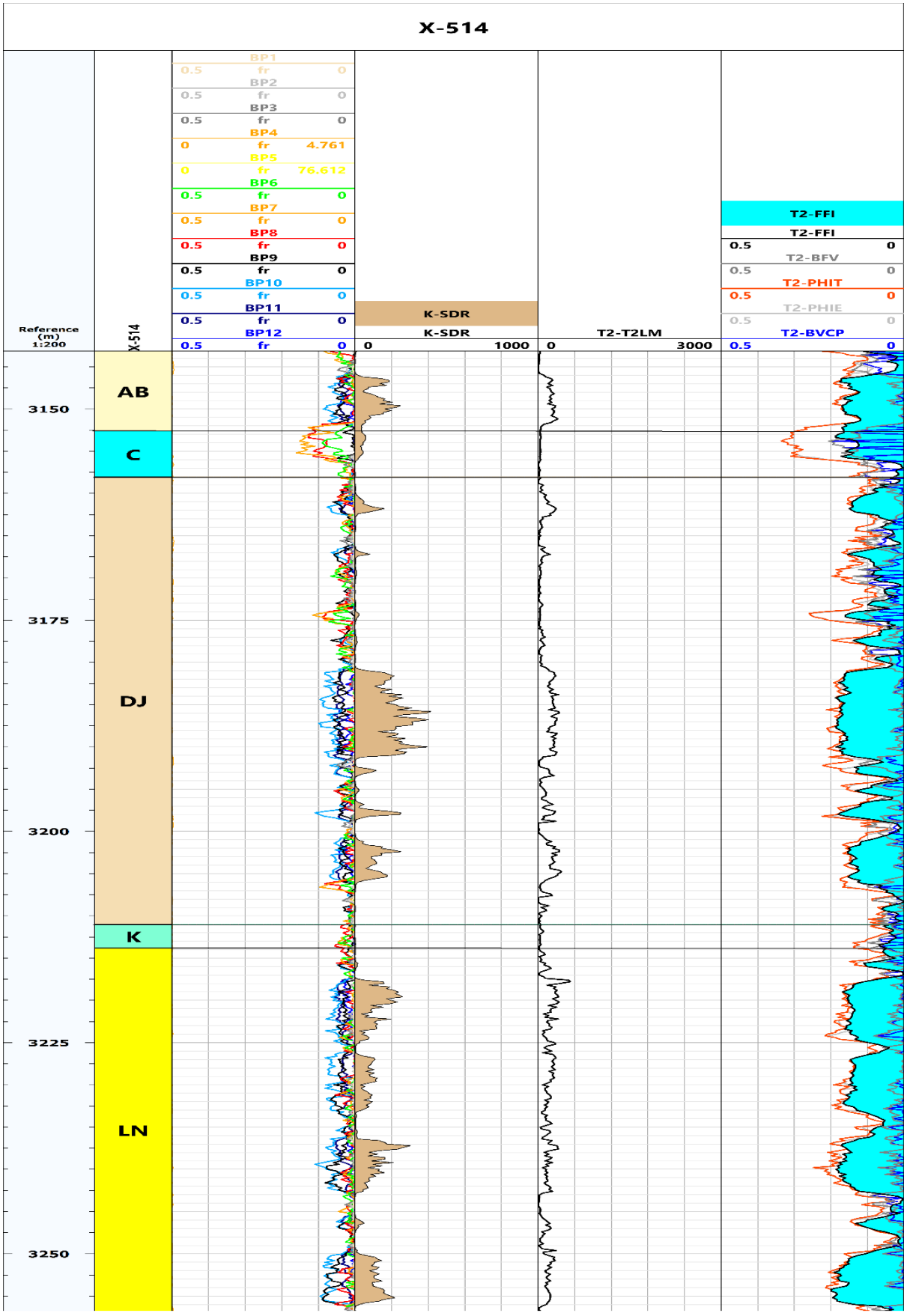

Fig.10. Nuclear magnetic resonance (NMR) for well X-515 showing petrophysical properties

Reference

Abdul-Majeed, Y.N., Ramadhan, A.A., Mahmood, A.J., 2020. Petrophysical Properties and well log interpretations of Tertiary reservoir in Khabaz Oil Field/Northern Iraq. Journal of Engineering 26, 18–34. https://doi.org/10.31026/j.eng.2020.06.02

Abdulnaby, W., 2019. Structural geology and neotectonics of Iraq, Northwest Zagros, in: Developments in Structural Geology and Tectonics. Elsevier, 53–73. https://doi.org/10.1016/B978-0-12-815048-1.00004-4

Al-Aradi, H.T., Alnajm, F.M., Al-Khafaji, A.J., 2022. Reservoir properties of the upper sand member of the Zubair Formation in North Rumaila Oil Field. Iraqi Geological Journal, 55(1C), 97–111. http://dx.doi.org/10.46717/igj.55.1C.8Ms-2022-03-27

Al-Jaberi, M.H., A-Jafar, M.K., 2020. Elements distribution for the upper sandstone member of the Zubair Formation in Zubair oil field, southern Iraq. Iraqi Geological Journal, 53(1E), 55–74. https://doi.org/10.46717/igj.53.1E.5Ry-2020-07-05

Al-Jaberi, M.H., Al-Mayyahi, H.K., 2018. Wireline logging response and true core analysis of the upper shale member of Zubair Formation, Rumaila oilfield, Southern Iraq. Iraqi Geological Journal, 51(2), 28–40. https://doi.org/10.46717/igj.51.2.2Ms-2018-12-24

Almayahi, A.Z., Ajeel, Z.A., 2020. Tectonic development of Nahr Umr oil field, southeastern Iraq: inferences from seismic reflection and borehole data. Arabian Journal of Geosciences, 13, 641. https://doi.org/10.1007/s12517-020-05663-6

Al-Samer, H.A., Al-Najm, F.M., 2024. Petrophysical and statistical analysis of main pay of the Zubair Formation in South Rumaila Oil Field. Iraqi Journal of Science 210–222. DOI:10.24996/ijs.2024.65.1.19

Archie, G.E., 1942. The electrical resistivity log as an aid in determining some reservoir characteristics. Transactions of the AIME, 146, 54–62. https://doi.org/10.2118/942054-G

Chafeet, H.A., Handhal, A.M., 2023. Using mud gas while drilling analysis to predict reservoir fluid characteristics of the Zubair reservoir in north Rumaila field, southern Iraq. Model. Earth Syst. Environ. 9, 3305–3328. https://doi.org/10.1007/s40808-023-01692-8

Doveton, J.H., Prensky, S.E., 1992. Geological applications of wireline logs: a synopsis of developments and trends. The Log Analyst 33, 286–303.

Elahifar, B., Esmaeili, A., Fruhwirth, R.K., Thonhauser, G., 2012. Accuracy of ultrasonic sensor in caliper log, in: 2012 IEEE International Instrumentation and Measurement Technology Conference Proceedings. Institute of Electrical and Electronics Engineers, 449–453. DOI:10.1109/I2MTC.2012.6229478

Handhal, A.M., Jawad, S.M., Al-Abadi, A.M., 2019. GIS-based machine learning models for mapping tar mat zones in upper part (DJ unit) of Zubair Formation in the north Rumaila supergiant oil field, southern Iraq. Journal of Petroleum Science and Engineering 178, 559–574. https://doi.org/10.1016/j.petrol.2019.03.071

Handhal, A.M., Al-Abadi, A.M., Chafeet, H.E., Ismail, M.J., 2020. Prediction of total organic carbon at Rumaila oil field, Southern Iraq using conventional well logs and machine learning algorithms. Marine and Petroleum Geology, 116, 104347. https://doi.org/10.1016/j.marpetgeo.2020.104347

Hasoon, S.K., Farman, G.M., 2024. A comprehensive review for integrating petrophysical properties, rock typing, and geological modeling for enhanced reservoir characterization. Journal of Engineering 30, 69–101. DOI: 10.31026/j.eng.2024.10.05

Horsfall, O.I., Uko, E.D., Tamunobereton-Ari, I., 2013. Comparative analysis of sonic and neutron-density logs for porosity determination in the South-eastern Niger Delta Basin, Nigeria. American Journal of Scientific and Industrial Research 4, 261–271. DOI: 10.5251/ajsir.2013.4.3.261.271

Ismail, M.J., Ettensohn, F.R., Handhal, A.M., Al-Abadi, A., 2021. Facies analysis of the Middle Cretaceous Mishrif Formation in southern Iraq borehole image logs and core thin-sections as a tool. Marine and Petroleum Geology 133, 105324. https://doi.org/10.1016/j.marpetgeo.2021.105324

Jaffar, H.M., 2018. Structural Geology of Rumaila Oilfield in Southern Iraq from Well Logs and Seismic Data, Unpub. M. Sc. theses, University of Basrah.

Kamel, M.H., Mabrouk, W.M., 2003. Estimation of shale volume using a combination of the three porosity logs. Journal of Petroleum Science and Engineering 40, 145–157. https://doi.org/10.1016/S0920-4105(03)00120-7.

Kamel, M.H., Mohamed, M.M., 2006. Effective porosity determination in clean/shaly formations from acoustic logs with applications. Journal of Petroleum Science and Engineering 51, 267–274. https://doi.org/10.1016/j.petrol.2006.01.007

Liu, H., 2017. Principles and Applications of Well Logging, Springer Mineralogy. Springer Berlin Heidelberg, Berlin, Heidelberg. https://doi.org/10.1007/978-3-662-53383-3

Macini, P., Mesini, E., 2008. Petrophysics and Reservoir Characteristics, in: Petroleum Engineering-Upstream. Eolss, 1–20.

Mitchell, J., Chandrasekera, T.C., Holland, D.J., Gladden, L.F., Fordham, E.J., 2013. Magnetic resonance imaging in laboratory petrophysical core analysis. Physics Reports 526, 165–225. https://doi.org/10.1016/j.physrep.2013.01.003

Mohammed, W.J., Al-Jawad, M.S., Al-Shamma, D.A., 2010. Reservoir flow simulation study for a sector in main pay-South Rumaila oil field, in Society of Petroleum Engineers Oil and Gas India Conference and Exhibition? SPE, SPE-126427. https://doi.org/10.2118/126427-MS

Paske, W.C., Mack, S.G., Rao, M.V., Spross, L., Twist, J.R., 1990. Measurement of hole size while drilling, in: SPWLA Annual Logging Symposium. Society of Petrophysicists and Well Log Analysts, SPWLA-1990.

Simandoux, P., 1963. Mesures dielectriques en milieu poreux, application a mesure des saturations en eau, Etude du Comportment des massifs Argileux. Revue de l'Institut Français du Pétrole, n Hors-Série 193–215.

Sissakian, V.K., 2013. Geological evolution of the Iraqi Mesopotamia Foredeep, inner platform and near surroundings of the Arabian Plate. Journal of Asian Earth Sciences 72, 152–163. https://doi.org/10.1016/j.jseaes.2012.09.032.

Spain, D.R., 1992. Petrophysical evaluation of a slope fan/basin-floor fan complex: Cherry Canyon Formation, Ward County, Texas. American Association of Petroleum Geologists Bulletin 76, 805–827.

Stick, Jr, J.C., Hartline, R., 1962. A review of current techniques in gamma-ray and neutron log interpretation. Journal of Petroleum Technology 14, 233–241.

Szabó, N.P., 2011. Shale volume estimation based on the factor analysis of well-logging data. Acta Geophys. 59, 935–953. https://doi.org/10.2478/s11600-011-0034-0

Watson, A.T., Chang, C.P., 1997. Characterizing porous media with NMR methods. Progress in Nuclear Magnetic Resonance Spectroscopy 31, 343–386. https://doi.org/10.1016/S0079-6565(97)00053-8

Wells, M., Morton, A., Frei, D., 2017. Provenance of Lower Cretaceous clastic reservoirs in the Middle East. Journal of the Geological Society (JGS), 174, 1048–1061. https://doi.org/10.1144/jgs2017-013

Wyllie, M.R.J., Gregory, A.R., Gardner, G.H.F., 1958. An experimental investigation of factors affecting elastic wave velocities in porous media. Geophysics, 23, 459–493. https://doi.org/10.1190/1.1438493